ARGONNE NATIONAL LABORATORY
9700 South Cass Avenue
Argonne, Illinois 60439

A Mixed-Integer PDE-Constrained Optimization Formulation for Electromagnetic Cloaking

Ryan H. Vogt, Sven Leyffer, and Todd Munson

Mathematics and Computer Science Division

Preprint ANL/MCS-P9277-0120

January 2020

[1]This material was based upon work supported by the U.S. Department of Energy, Office of Science, Office of Advanced Scientific Computing Research, Scientific Discovery through Advanced Computing (SciDAC) program through the FASTMath Institute under Contract DE-AC02-06CH11357 at Argonne National Laboratory. This work was also supported by the U.S. Department of Energy through grant DE-FG02-05ER25694.

A MIXED-INTEGER PDE-CONSTRAINED OPTIMIZATION FORMULATION FOR ELECTROMAGNETIC CLOAKING *

RYAN H. VOGT†, SVEN LEYFFER‡, AND TODD MUNSON§

Abstract. We formulate a mixed-integer partial-differential equation constrained optimization problem for designing an electromagnetic cloak governed by the 2D Helmholtz equation with absorbing boundary conditions. Our formulation is an alternative to the topology optimization formulation of electromagnetic cloaking design. We extend the formulation to include uncertainty with respect to the angle of the incidence wave, and we develop a mixed-integer trust-region approach for solving both the deterministic and the uncertain formulation. We present detailed numerical results that show that our trust-region approach obtains effective cloaks.

Key words. PDE-constrained optimization, mixed-integer nonlinear optimization, Helmholtz equation, electromagnetic cloaking.

AMS subject classifications. 35J05, 49M37, 90C30

1 Introduction

Since the study of optics began, the ability to control the properties of light with materials found in nature has been limited. The introduction of metamaterials, which cannot be found in nature, made the creation of electromagnetic cloaks feasible and brought a strong interest to this field of study [17]. The goal of an electromagnetic cloak on an object is for the light to flow around the object, rather than being scattered by the object, causing the object to optically disappear. Numerical simulations and experiments reported in 2006 and 2007 highlighted advancements in the construction of electromagnetic cloaks [5, 7]; and experiments reported in [17] have established the first practical implementation of an electromagnetic cloak over a small-frequency band . While this cloak was unsuccessful in obtaining perfect cloaking of a copper cylinder, the experiments showed the ability to decrease the shadow of an object, getting closer to resembling empty space, thus reinforcing the theory of electromagnetic cloaking and the practicality of an implementation. In [6] the authors presented an in-depth summary of electromagnetic cloaking by means of metamaterials. Highlights include several key experiments, and also a discussion of future directions for electromagnetic cloaking, especially in the area of cloaking for a large frequency band, which has not yet been observed. Recently, experimental observations established the construction of electromagnetic cloaks which are not dependent on prior knowledge of the incidence wave [18].

In this paper, we study the design of electromagnetic cloaks by formulating and solving a mixed-integer partial-differential equation constrained optimization (MIPDECO) problem. The objective is to minimize the integral of the response in the region we wish to cloak. The constraints include a 2D Helmholtz equation with absorbing boundary conditions for each component of the complex-valued scattering

*Submitted to the editors January 29, 2020.

Funding: This material was based upon work supported by the U.S. Department of Energy, Office of Science, Office of Advanced Scientific Computing Research, Scientific Discovery through Advanced Computing (SciDAC) program through the FASTMath Institute under Contract DE-AC02-06CH11357 at Argonne National Laboratory. This work was also supported by the U.S. Department of Energy through grant DE-FG02-05ER25694.

†North Carolina State University, Department of Mathematics, rvogt2@ncsu.edu

‡Argonne National Laboratory, Mathematics and Computer Science Division, leyffer@mcs.anl.gov

§Argonne National Laboratory, Mathematics and Computer Science Division, tmunson@mcs.anl.gov

wave that are parameterized by the design of the electromagnetic cloak. The design is obtained by using binary variables that determine whether a cell in the system is filled with material or not. The cloak design depends on the region to cloak, the angle of the incidence wave, the cloaking material, and the wavenumber.

We extend the cloak design by including uncertainty with respect to the angle of attack, leading to a stochastic programming formulation where we minimize the expected value of the objective function with respect to a discrete set of angles.

We solve the resulting combinatorial optimization problem in two steps. The first step relaxes the binary variables, solves the relaxation, and applies a rounding heuristic to obtain an initial design. The second step consists of a set of trust-region iterations to improve upon the initial design. Our approach replaces the large-scale mixed-integer nonlinear program (MINLP) by a sequence of easier linear knapsack problems that can be solved in polynomial time.

Paper Outline. In Section 2 we define the infinite-dimensional electromagnetic cloaking problem for a nominal wave angle. We then extend this formulation to an optimization problem under uncertainty that can account for uncertainty in the angle of the incidence wave, and we compute sensitivities with respect to the design variables that are needed in our optimization approach. In Section 3 we derive a finite-dimensional optimal design problem by discretizing the PDE using a finite-element approach, resulting in a large-scale MINLP. Next, we present an approach to solve the relaxed MINLP. In Section 4 we motivate a simple rounding heuristic and describe our trust-region steepest-descent algorithm. We provide numerical experiments in Section 5 to demonstrate the success of our trust-region method, and we comment on the computational effort to solve our problems. We conclude with a brief summary in Section 6. Detailed numerical results are presented in the electronic supplement SM1.

2 Electromagnetic Cloaking Design

In this section we review the infinite-dimensional cloaking design problem. We extend the nominal design and propose a stochastic optimization formulation for the design under uncertainty. We also show how adjoints of the problems are derived. These adjoints are needed for the solution of the continuous relaxation and for our proposed trust-region method.

2.1 Formulation of the Nominal Electromagnetic Cloaking Problem

We consider the design of an electromagnetic cloak from [11], where we aim to determine the optimal topology. We let $D \subset \mathbb{R}^2$ be the computational domain and $D_0 \subset D$ be the part of the domain that we wish to cloak. We let $\widehat{D} \subset D - D_0$ be the subregion in which we can design the cloak and $\Omega \subset \widehat{D}$ be the topology of the cloak. The optimal topology is determined by solving the following topology optimization problem that aims to minimize the response due to the incidence wave in D_0 subject to the Helmholtz equation in D:

$$
\begin{aligned}
\underset{u,\Omega\subset\widehat{D}}{\text{minimize}} \quad & \frac{1}{2}\left\|u+\bar{u}_\theta\right\|_{2,D_0}^2 \\
\text{subject to} \quad & -\Delta u - k_0^2\big(1+q\mathbb{1}_\Omega\big)u = k_0^2\mathbb{1}_\Omega\bar{u}_\theta \quad \text{in } D \\
& \frac{\partial u}{\partial n} - ik_0 u = 0 \qquad\qquad\qquad\qquad\quad \text{on } \partial D,
\end{aligned}
\tag{2.1}
$$

where $i=\sqrt{-1}$, ∂D is the boundary of the computational domain and

$$
\bar{u}_\theta(x,y) = \exp(ik_0(x\cos(\theta)+y\sin(\theta))) \tag{2.2}
$$

is the incidence wave in direction $d = (\cos(\theta), \sin(\theta))$, with wave number k_0. The angle θ at which the incidence wave approaches the cloak is measured from the x-axis, and we refer to θ as the nominal angle of attack. The state variable u represents the electromagnetic field intensity, and the parameter q is the electromagnetic permitivity difference between Ω, the part of the cloak filled with material, and $\widehat{D} - \Omega$ the part of the cloak without material.

When manufacturing cloaks, there is typically a lower bound on the size of the features in the cloak, Ω. We partition the cloak Ω into a finite number of uniform squares, Ω_n, for $n = 1, \ldots, N$. We refer to this partition as the *control mesh* and assume that

$$\Omega = \bigcup_{n=1}^{N} \Omega_n \quad \text{and} \quad \left(\Omega_n \backslash \partial\Omega_n\right) \cap \left(\Omega_p \backslash \partial\Omega_p\right) = \varnothing \text{ for } n \neq p;$$

see Figure 1a for an illustration.

We represent the decision of whether or not to fill a square $\Omega_n \subset \Omega$ by a binary (control) variable $v_n \in \{0, 1\}$ for $n = 1, \ldots, N$, and we define the indicator function $\mathbb{1}_{\Omega_n}$ for Ω_n as

$$\mathbb{1}_{\Omega_n}(x, y) = \begin{cases} 1 & \text{if } (x, y) \in \Omega_n \\ 0 & \text{otherwise,} \end{cases} \tag{2.3}$$

for $n = 1...N$. The resulting reformulation of (2.1) can be rewritten as the MIPDECO

$$\begin{aligned} \underset{u,v,w}{\text{minimize}} \quad & \frac{1}{2}\|u + \bar{u}_\theta\|^2_{2,D_0} & \\ \text{subject to} \quad & -\Delta u - k_0^2(1 + qw)u = k_0^2 qw\bar{u}_\theta & \text{in } D \\ & \frac{\partial u}{\partial n} - ik_0 u = 0 & \text{on } \partial D \\ & w = \sum_{n=1}^{N} v_n \mathbb{1}_{\Omega_n \backslash \partial\Omega_n} & \\ & v_n \in \{0, 1\} & \forall n = 1, \ldots, N, \end{aligned} \tag{2.4}$$

where the defined control, w, now takes the place of the topological variable, Ω. In this formulation, we have a fixed finite number of binary variables v_n that represent the design. Because $u, \bar{u}_\theta : \mathbb{R}^2 \to \mathbb{C}$ is complex valued, we split u and $\bar{u}_\theta$ into its real and imaginary parts, $u = u_{\text{Re}} + iu_{\text{Im}}$, resulting in two separate PDEs for the real and the imaginary part, respectively.

In general, we have an $m \times m$ control mesh made up of $N = m^2$ binary variables. We illustrate a sample design in Figure 1a, where red indicates material and blue indicates no material.

2.2 Optimal Design for Electromagnetic Cloaking under Uncertainty

Here, we extend the optimal design problem to account for uncertainty in the incidence angle or angle of attack, θ. We formulate an optimization problem to create a design that can effectively cloak a given region even if the incidence angle of the wave changes.

To account for uncertainty in the design, we generalize problem (2.4) to allow a range of incidence angles θ and we regard the incidence angle as a random variable. We can then formulate an optimization problem that minimizes, for example, the expected value of the effectiveness of the cloak. We let $(\Theta, \mathcal{F}, P)$ be a triple of sample

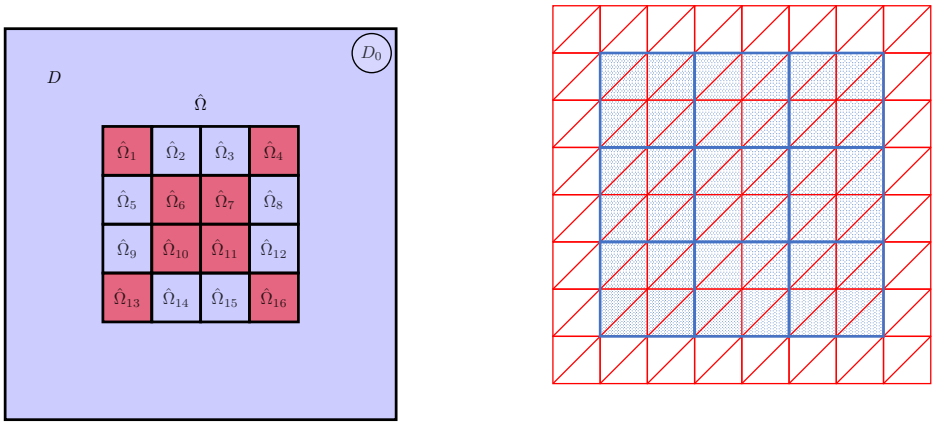

(a) Cloak Illustration

(b) Finite-Element Grid Illustration

Fig. 1: 1a: Illustration of a 4×4 grid of control elements in which the goal is to cloak the region D_0, in this case a circle in the top right corner of the domain. 1b: Illustration of the state and adjoint finite-element method (FEM) discretization. Each control element (blue) is composed of eight triangular finite elements. In the FEM approach we represent each control element as a constant with value v_n. The state and adjoint variables are defined on the finite-element mesh.

space, σ-algebra, and probability measure, and we formulate the following stochastic optimization problem:

$$
\begin{aligned}
\underset{u,v,w}{\text{minimize}} \quad & \mathcal{J}(u,v,w) = \mathbb{E}_\theta\left[\frac{1}{2}\|u_\theta + \bar{u}_\theta\|^2_{2,D_0}\right] \\
\text{subject to} \quad & -\Delta u_\theta - k_0^2(1+qw)u_\theta = k_0^2 qw\bar{u}_\theta && \text{in } D,\ \forall\theta\in\Theta \\
& \frac{\partial u_\theta}{\partial n} - ik_0 u_\theta = 0 && \text{on } \partial D,\ \forall\theta\in\Theta \\
& w = \sum_{n=1}^{N} v_n \mathbb{1}_{\Omega_n\setminus\partial\Omega_n} \\
& v_n = \{0,1\} && \forall n = 1,\dots,N,
\end{aligned}
\tag{2.5}
$$

where $\mathbb{E}_\theta[\cdot]$ is the expectation with respect to the random variable θ and $u_\theta = u_\theta(v)$ is the solution of the PDE for a given control, v, and incidence angle, θ. Problem (2.5) has a structure similar to that of a two-stage stochastic program if we interpret the controls w and v as the first-stage decision variables, and the states u_θ as the second-stage variables. However, there is no optimization in the second stage because w, v, and θ uniquely determine u_θ. To approximate the expectation in (2.5), we select a finite set of s angles denoted by the set $\Theta(s) \subset \Theta$, for example,

$$
\Theta(s) = \left\{\theta_j \middle|\ \theta_j = \frac{\pi j}{2s}, j = 0,\dots,s\right\},
$$

and we replace the expectation by the sample average mean. We assume that each θ_j

has a probability P_j of occurring, and we assume that all angles of attack are equally likely, $P_j = \frac{1}{|\Theta(s)|}$ (though this assumption is readily relaxed). We can interpret $\Theta(s)$ as a discretization of a uniform distribution over the interval of interest. We now rewrite our cloaking optimization problem for the finite set $\Theta(s)$ as

(2.6)

$$\begin{aligned}
\underset{u^{(j)},v,w}{\text{minimize}} \quad & \mathcal{J}(u^{(j)},v,w) = \frac{1}{2|\Theta(s)|}\sum_{j=0}^{s} \|u^{(j)} + \bar{u}^{(j)}\|^2_{2,D_0} \\
\text{subject to} \quad & -\Delta u^{(j)} - k_0^2(1+qw)u^{(j)} = k_0^2 qw\bar{u}^{(j)} && \text{in } D,\ \forall j = 0,\dots,s \\
& \frac{\partial u^{(j)}}{\partial n} - ik_0 u^{(j)} = 0 && \text{on } \partial D,\ \forall j = 0,\dots,s \\
& w = \sum_{n=1}^{N} v_n \mathbb{1}_{\Omega_n \setminus \partial\Omega_n} \\
& v_n = \{0,1\} && \forall n = 1,\dots,N.
\end{aligned}$$

where $u^{(j)}$ is the state corresponding to the jth scenario, θ_j, and the incidence wave associated with θ_j is defined as

$$\bar{u}^{(j)}(x,y) = \exp\left(ik_0(x\cos(\theta_j) + y\sin(\theta_j))\right),\ \forall j = 0,\dots,s. \tag{2.7}$$

This stochastic program has $2|\Theta(s)|$ state variables and $2|\Theta(s)|$ adjoint variables. The evaluation of the objective function and gradient of (2.5) requires the solution of $4|\Theta(s)|$ PDEs for each fixed v.

2.3 Weak Adjoint and Gradient Equations Our method for solving (2.6) is based on solving the continuous relaxation followed by a rounding step and an incremental trust-region improvement algorithm. Both steps require computing gradients with respect to the control variables v. Here, we present the derivation of the weak state and weak adjoint equation for the uncertain problem (the derivation for the easier nominal problem follows in a similar way). In addition we provide the strong gradient derivation for (2.5) using the adjoint approach for calculating the gradient for the continuous relaxation ($0 \leqslant v \leqslant 1$). We begin by formally defining the strong Lagrangian $\mathcal{L}$ of (2.6) as

$$\begin{aligned}
&\mathcal{L}(u^{(j)}_{\mathrm{Re}}, u^{(j)}_{\mathrm{Im}}, v; \lambda^{(j)}_{\mathrm{Re}}, \lambda^{(j)}_{\mathrm{Im}}, \theta) \\
&= \frac{1}{2|\Theta(s)|}\Bigg(\sum_{j=0}^{s}\Big(\int_{D_0}\left(u^{(j)}_{\mathrm{Re}} + \bar{u}^{(j)}_{\mathrm{Re}}\right)^2 + \left(u^{(j)}_{\mathrm{Im}} + \bar{u}^{(j)}_{\mathrm{Im}}\right)^2 dD_0\Bigg) \\
&+ \sum_{j=0}^{s}\left\langle \lambda^{(j)}_{\mathrm{Re}}, \left(-\Delta u^{(j)}_{\mathrm{Re}} - k_0^2(1+qw)u^{(j)}_{\mathrm{Re}} - k_0^2 qw\bar{u}^{(j)}_{\mathrm{Re}}\right)\right\rangle_{L^2(D)} \\
&+ \sum_{j=0}^{s}\left\langle \lambda^{(j)}_{\mathrm{Im}}, \left(-\Delta u^{(j)}_{\mathrm{Im}} - k_0^2(1+qw)u^{(j)}_{\mathrm{Im}} - k_0^2 qw\bar{u}^{(j)}_{\mathrm{Im}}\right)\right\rangle_{L^2(D)},
\end{aligned} \tag{2.8}$$

where $\langle\cdot,\cdot\rangle_{L^2(D)}$ is the L^2 inner product over D and $\lambda^{(j)}_{\mathrm{Re}}, \lambda^{(j)}_{\mathrm{Im}}$ are the adjoint variables for the jth real and imaginary state equation respectively. In (2.8) the strong Lagrangian is defined: we assume that the pairs $u^{(j)}_{\mathrm{Re}}, u^{(j)}_{\mathrm{Im}} \in C^2(D)$ are twice continuously differentiable. We weaken this regularity assumption because we intend to search for weak solutions with the finite-element method. Next, we derive the weak

form of the Lagrangian by applying Green's theorem to the two constraint terms:

$$
\begin{aligned}
&\sum_{j=0}^{s} \left\langle \lambda_{\mathrm{Re}}^{(j)}, \left(-\Delta u_{\mathrm{Re}}^{(j)} - k_0^2(1+qw)u_{\mathrm{Re}}^{(j)} - k_0^2 qw\bar{u}_{\mathrm{Re}}^{(j)}\right)\right\rangle_{L^2(D)} \\
&= \sum_{j=0}^{s}\left[\int_D \lambda_{\mathrm{Re}}^{(j)}\left(-\Delta u_{\mathrm{Re}}^{(j)} - k_0^2(1+qw)u_{\mathrm{Re}}^{(j)} - k_0^2 qw\bar{u}_{\mathrm{Re}}^{(j)}\right) dD\right] \\
&= \sum_{j=0}^{s}\left[\int_D \nabla u_{\mathrm{Re}}^{(j)}\cdot\nabla\lambda_{\mathrm{Re}}^{(j)} dD + \int_{\partial D} k_0 u_{\mathrm{Im}}^{(j)}\lambda_{\mathrm{Re}}^{(j)} d\partial D\right. \\
&\left. - \int_D \lambda_{\mathrm{Re}}^{(j)}\left(k_0^2(1+qw)u_{\mathrm{Re}}^{(j)} + k_0^2 qw\bar{u}_{\mathrm{Re}}^{(j)}\right) dD\right]
\end{aligned} \tag{2.9}
$$

and

$$
\begin{aligned}
&\sum_{j=0}^{s}\left[\left\langle \lambda_{\mathrm{Im}}^{(j)}, \left(-\Delta u_{\mathrm{Im}}^{(j)} - k_0^2(1+qw)u_{\mathrm{Im}}^{(j)} - k_0^2 qw\bar{u}_{\mathrm{Im}}^{(j)}\right)\right\rangle_{L^2(D)}\right] \\
&= \sum_{j=0}^{s}\left[\int_D \lambda_{\mathrm{Im}}^{(j)}\big(-\Delta u_{\mathrm{Im}}^{(j)} - k_0^2(1+qw)u_{\mathrm{Im}}^{(j)} - k_0^2 qw\bar{u}_{\mathrm{Im}}^{(j)} dD\big)\right] \\
&= \sum_{j=0}^{s}\left[\int_D \nabla u_{\mathrm{Im}}^{(j)}\cdot\nabla\lambda_{\mathrm{Im}}^{(j)} dD - \int_{\partial D} k_0 u_{\mathrm{Re}}^{(j)}\lambda_{\mathrm{Im}}^{(j)} d\partial D\right. \\
&\left. - \int_D \lambda_{\mathrm{Im}}^{(j)}\left(k_0^2(1+qw)u_{\mathrm{Im}}^{(j)} + k_0^2 qw\bar{u}_{\mathrm{Im}}^{(j)}\right) dD\right].
\end{aligned} \tag{2.10}
$$

We substitute (2.9) and (2.10) into (2.8) and obtain the weak Lagrangian:

$$
\begin{aligned}
&\mathcal{L}(u_{\mathrm{Re}}^{(j)}, u_{\mathrm{Im}}^{(j)}, v, \lambda_{\mathrm{Re}}^{(j)}, \lambda_{\mathrm{Im}}^{(j)}, \theta) \\
&= \frac{1}{2|\Theta(s)|}\left(\sum_{j=0}^{s}\big(\int_{D_0}\big(u_{\mathrm{Re}}^{(j)} + \bar{u}_{\mathrm{Re}}^{(j)}\big)^2 + \big(u_{\mathrm{Im}}^{(j)} + \bar{u}_{\mathrm{Im}}^{(j)}\big)^2 dD_0\big)\right) \\
&+ \sum_{j=0}^{s}\left[\int_D \nabla u_{\mathrm{Re}}^{(j)}\cdot\nabla\lambda_{\mathrm{Re}}^{(j)} dD + \int_{\partial D} k_0 u_{\mathrm{Im}}^{(j)}\lambda_{\mathrm{Re}}^{(j)} d\partial D\right. \\
&\qquad \left. - \int_D \big[\lambda_{\mathrm{Re}}^{(j)}\big[k_0^2(1+qw)u_{\mathrm{Re}}^{(j)} + k_0^2 qw\bar{u}_{\mathrm{Re}}^{(j)}\big]\big] dD\right] \\
&+ \sum_{j=0}^{s}\left[\int_D \nabla u_{\mathrm{Im}}^{(j)}\cdot\nabla\lambda_{\mathrm{Im}}^{(j)} dD - \int_{\partial D} k_0 u_{\mathrm{Re}}^{(j)}\lambda_{\mathrm{Im}}^{(j)} d\partial D\right. \\
&\qquad \left. - \int_D \big[\lambda_{\mathrm{Im}}^{(j)}\big[k_0^2(1+qw)u_{\mathrm{Im}}^{(j)} + k_0^2 qw\bar{u}_{\mathrm{Im}}^{(j)}\big]\big] dD\right].
\end{aligned} \tag{2.11}
$$

In the final form (2.11), we assume that $u_{\mathrm{Re}}^{(j)}, u_{\mathrm{Im}}^{(j)} \in H^1(D)$, where $H^1(D) := W^{1,2}$ is the Sobolev space of all functions that are $L^2(D)$ (square integrable) and whose weak derivative in the sense of distributions is also in $L^2(D)$. To find the sensitivities of the objective function, $\mathcal{J}$, with respect to v, we exploit the fact that there exists a unique w for any choice of v and that (under suitable conditions on k_0) there exists a unique u for any v. We start by deriving the weak state equations, which are obtained by taking variations with respect to $\tilde{\lambda}_{\mathrm{Re}}^{(j)}, \tilde{\lambda}_{\mathrm{Im}}^{(j)}$ for all $j = 0, ..., s$:

$$
0 = \mathcal{L}_{\lambda_{\mathrm{Re}}^{(j)}}[\tilde{\lambda}_{\mathrm{Re}}^{(j)}] = \int_D \nabla u_{\mathrm{Re}}^{(j)}\cdot\nabla\tilde{\lambda}_{\mathrm{Re}}^{(j)} dD + \int_{\partial D} k_0 u_{\mathrm{Im}}^{(j)}\tilde{\lambda}_{\mathrm{Re}}^{(j)} d\partial D \tag{2.12}
$$

$$- \int_D \tilde{\lambda}_{\mathrm{Re}}^{(j)} \big[k_0^2(1+qw)u_{\mathrm{Re}}^{(j)} + k_0^2 qw\bar{u}_{\mathrm{Re}}^{(j)}\big]dD, \qquad \forall \tilde{\lambda}_{\mathrm{Re}}^{(j)} \in H^1(D)$$

$$0 = \mathcal{L}_{\lambda_{\mathrm{Im}}^{(j)}}[\tilde{\lambda}_{\mathrm{Im}}^{(j)}] = \int_D \nabla u_{\mathrm{Im}}^{(j)} \cdot \nabla \tilde{\lambda}_{\mathrm{Im}}^{(j)} dD - \int_{\partial D} k_0 u_{\mathrm{Re}}^{(j)} \tilde{\lambda}_{\mathrm{Im}}^{(j)} d\partial D \tag{2.13}$$

$$- \int_D \tilde{\lambda}_{\mathrm{Im}}^{(j)} \big[k_0^2(1+qw)u_{\mathrm{Im}}^{(j)} + k_0^2 qw\bar{u}_{\mathrm{Im}}^{(j)}\big]dD, \qquad \forall \tilde{\lambda}_{\mathrm{Im}}^{(j)} \in H^1(D)$$

We note that the weak state equation pair has a unique solution in $H^1(D)$ [11]. Once we have solved this state equation pair, we can calculate the adjoint pairs, $(\lambda_{\mathrm{Re}}^j, \lambda_{\mathrm{Im}}^j)$, by solving the weak adjoint equations obtained by taking variations with respect to $\tilde{u}_{\mathrm{Re}}^{(j)}, \tilde{u}_{\mathrm{Im}}^{(j)}$ for all $j = 0, ..., s$:

$$0 = \mathcal{L}_{u_{\mathrm{Re}}^{(j)}}[\tilde{u}_{\mathrm{Re}}^{(j)}] = \frac{1}{|\Theta(s)|} \int_{D_0} \big(u_{\mathrm{Re}}^{(j)} + \bar{u}_{\mathrm{Re}}^{(j)}\big)\tilde{u}_{\mathrm{Re}}^{(j)} dD_0$$

$$+ \int_D \nabla \tilde{u}_{\mathrm{Re}}^{(j)} \cdot \nabla \lambda_{\mathrm{Re}}^{(j)} dD - \int_D \lambda_{\mathrm{Re}}^{(j)} k_0^2(1+qw)\tilde{u}_{\mathrm{Re}}^{(j)} dD \tag{2.14}$$

$$- \int_{\partial D} k_0 \tilde{u}_{\mathrm{Re}}^{(j)} \lambda_{\mathrm{Im}}^{(j)} d\partial D, \qquad \forall \tilde{u}_{\mathrm{Re}}^{(j)} \in H^1(D),$$

$$0 = \mathcal{L}_{u_{\mathrm{Im}}^{(j)}}[\tilde{u}_{\mathrm{Im}}^{(j)}] = \frac{1}{|\Theta(s)|} \int_{D_0} \big(u_{\mathrm{Im}}^{(j)} + \bar{u}_{\mathrm{Im}}^{(j)}\big)\tilde{u}_{\mathrm{Im}}^{(j)} dD_0$$

$$+ \int_D \nabla \tilde{u}_{\mathrm{Im}}^{(j)} \cdot \nabla \lambda_{\mathrm{Im}}^{(j)} dD - \int_D \lambda_{\mathrm{Im}}^{(j)} k_0^2(1+qw)\tilde{u}_{\mathrm{Im}}^{(j)} dD \tag{2.15}$$

$$+ \int_{\partial D} k_0 \tilde{u}_{\mathrm{Im}}^{(j)} \lambda_{\mathrm{Re}}^{(j)} d\partial D, \qquad \forall \tilde{u}_{\mathrm{Im}}^{(j)} \in H^1(D).$$

The proof for the existence and uniqueness of the solution to general elliptic equations with Robin boundary conditions in $H^1(D)$ can be found in [16] and extends to the adjoint equation pair, which differs from the state equation pair only in its source term. An argument similar to [11] can then be applied to show the existence and uniqueness of the solutions.

After we have calculated the state and adjoint variables for all scenarios, we can assemble the nth component of the gradient of the Lagrangian with respect to v_n:

$$\big(\nabla_v \mathcal{L}\big)_n = -\sum_{j=0}^{s} \int_{\hat{\Omega}_n} \Big(k_0^2 q(u_{\mathrm{Re}}^{(j)}\lambda_{\mathrm{Re}}^{(j)} + u_{\mathrm{Im}}^{(j)}\lambda_{\mathrm{Im}}^{(j)}) + k_0^2 q(\bar{u}_{\mathrm{Re}}^{(j)}\lambda_{\mathrm{Re}}^{(j)} + \bar{u}_{\mathrm{Im}}^{(j)}\lambda_{\mathrm{Im}}^{(j)})\Big) d\hat{\Omega}_n. \tag{2.16}$$

One can show, as illustrated in [19, Lemma 2.30], that the weak gradient equation $\mathcal{L}_v[\tilde{v}]$ satisfies

$$\mathcal{L}_v[\tilde{v}] = \langle \nabla_v \mathcal{L}, \tilde{v} \rangle_{\mathbb{R}^N} = \langle \hat{\mathcal{J}}'(v), \tilde{v} \rangle_{\mathbb{R}^N} \quad \forall \tilde{v} \in \mathbb{R}^N. \tag{2.17}$$

Because v is a continuous finite-dimensional decision variable during the relaxation process, we can produce the strong gradient (which is also the weak gradient) by differentiating (2.11) with respect to v. Following [19, Lemma 2.21],

$$\Big(\hat{\mathcal{J}}'(v^*)\Big)^T (v - v^*) \geqslant 0 \quad \forall v \in V = \{v : 0 \leqslant v \leqslant 1, v \in \mathbb{R}^N\} \tag{2.18}$$

are the necessary optimality conditions of the reduced space formulation,

$$\underset{0 \leqslant v \leqslant 1}{\text{minimize}} \quad \hat{\mathcal{J}}(v) = \frac{1}{2|\Theta(s)|} \sum_{j=0}^{s} \|S_{\theta_j}(v) + \bar{u}^{(j)}\|_{2,D_0}^2, \tag{2.19}$$

with S_{θ_j} being the solution operator $S_j : v \to u_j$ for incidence angle θ_j.

3 Solving the Continuous Optimal Design Problem In this section we describe our discretization and then show how we solve the continuous design problem using a reduced-space method.

3.1 Discretization of State and Adjoint Equations Here we show how to solve discretizations of the state and adjoint PDEs and compute (discretized) gradients that can be used in a reduced-space approach. To solve the state and adjoint PDEs we use a Galerkin FEM [12]. We decompose our physical domain D into a computational domain made up of uniform triangle elements, E_i, with length and height h as illustrated in Figure 1b, such that

$$D = \bigcup_i E_i \quad \text{and} \quad \big(E_i \backslash \partial E_i\big) \cap \big(E_j \backslash \partial E_j\big) = \varnothing, \ \forall i \neq j. \tag{3.1}$$

We also assume that each control element Ω_n covers a fixed number of finite elements E_i, as shown in Figure 1b.

We construct an approximate solution to the state and adjoint variables using piecewise linear test functions on our finite elements, giving linear test functions that have compact support on their element. We then approximate the solution by a linear combination of the test functions for the jth scenario:

$$u_{\text{Re}}^{h,j} = \sum_{i=1}^{R(h)} \mathbf{u}_{\text{Re}}^{i,j}\phi_i, \quad u_{\text{Im}}^{h,j} = \sum_{i=1}^{R(h)} \mathbf{u}_{\text{Im}}^{i,j}\phi_i, \quad \lambda_{\text{Re}}^{h,j} = \sum_{i=1}^{R(h)} \boldsymbol{\lambda}_{\text{Re}}^{i,j}\phi_i, \quad \lambda_{\text{Im}}^{h,j} = \sum_{i=1}^{R(h)} \boldsymbol{\lambda}_{\text{Im}}^{i,j}\phi_i, \tag{3.2}$$

where $\mathbf{u}_{\text{Re}}^j, \mathbf{u}_{\text{Im}}^j, \boldsymbol{\lambda}_{\text{Re}}^j$, and $\boldsymbol{\lambda}_{\text{Im}}^j$ are the coefficient vectors of our expansion that are determined by the FEM (we use boldface to indicate finite-dimensional vectors in the remainder). Here, $R(h)$ is the number of elements in the discretization for a fixed step size h, and we choose piecewise linear test functions.

Given a v (and hence, w), we substitute (3.2) into (2.12), (2.13), (2.14), and (2.15). This approach allows us to find the coefficients by solving a linear system of equations that defines our approximate solution to the state and adjoint equations over the domain D. The resulting linear systems of equations (for fixed v) is obtained by substituting our trial solution into the real and imaginary state equations

$$\begin{bmatrix} \mathbf{A}(v) & \mathbf{B}(v) \\ -\mathbf{B}(v) & \mathbf{A}(v) \end{bmatrix} \begin{bmatrix} \mathbf{u}_{\text{Re}}^j \\ \mathbf{u}_{\text{Im}}^j \end{bmatrix} = \begin{bmatrix} \mathbf{f}_{\text{Re}}^j(v) \\ \mathbf{f}_{\mathbf{Im}}^j(v) \end{bmatrix} \tag{3.3}$$

for the jth incidence angle, where

$$\Big[\mathbf{A}(v)\Big]_{i,l} = \int_D \nabla\phi_i \cdot \nabla\phi_l dD + \int_{\partial D} k_0 \phi_i \phi_l d\partial D - \int_D k_0^2 \left(1 + q\left(\sum_{n=1}^N v_n \mathbb{1}_{\Omega_n \backslash \partial\Omega_n}\right)\right)\phi_i\phi_l dD,$$

$$\Big[\mathbf{B}(v)\Big]_{i,l} = \int_{\partial D} k_0 \phi_i \phi_l d\partial D,$$

and

$$\Big[\mathbf{f}_{\text{Re}}^j(v)\Big]_i = \int_D k_0^2 q\left(\sum_{n=1}^N v_n \mathbb{1}_{\Omega_n \backslash \partial\Omega_n}\right)\bar{u}_{\text{Re}}^{(j)}\phi_i dD.$$

We note $\mathbf{f}_{\text{Im}}^j$ is defined analogously by replacing $\bar{u}_{\text{Re}}^{(j)}$ by $\bar{u}_{\text{Im}}^{(j)}$.

Next we write down the systems for the adjoint variables associated with the real and imaginary adjoint equations. We note that the weak adjoint equations depend on the solution to the state equations. In the discretized adjoint equations we use the discretized solution found by solving the state equations as an approximation to the state. The system for the adjoint variables is

$$\begin{bmatrix} \mathbf{A}(v) & -\mathbf{B}(v) \\ \mathbf{B}(v) & \mathbf{A}(v) \end{bmatrix} \begin{bmatrix} \boldsymbol{\lambda}^j_{\mathrm{Re}} \\ \boldsymbol{\lambda}^j_{\mathrm{Im}} \end{bmatrix} = \begin{bmatrix} \mathbf{g}^j_{\mathrm{Re}}(v) \\ \mathbf{g}^j_{\mathbf{Im}}(v) \end{bmatrix} \tag{3.4}$$

for the jth incidence angle, where

$$\left[\mathbf{g}^j_{\mathrm{Re}}(u)\right]_i = -\frac{1}{|\Theta(s)|}\int_{D_0} \left(u^{h,j}_{\mathrm{Re}} + \bar{u}^{(j)}_{\mathrm{Re}}\right)\phi_i dD_0$$

and

$$\left[\mathbf{g}^j_{\mathrm{Im}}(u)\right]_i = -\frac{1}{|\Theta(s)|}\int_{D_0} \left(u^{h,j}_{\mathrm{Im}} + \bar{u}^{(j)}_{\mathrm{Im}}\right)\phi_i dD_0$$

are affine functions of the states, u.

Once we have found the solution to the state and adjoint equations, we construct an approximation of the nth component of the reduced gradient, $\left(\mathcal{J}'(v)\right)^h_n$, by using a tensorized two-point Gauss-Legendre quadrature rule to approximate

$$\left(\nabla_v \hat{J}^h(v)\right)_n = -\sum_{j=0}^{s}\int_{\hat{\Omega}_n}\left(k_0^2 q(u^{h,j}_{\mathrm{Re}}\lambda^{h,j}_{\mathrm{Re}} + u^{h,j}_{\mathrm{Im}}\lambda^{h,j}_{\mathrm{Im}}) + k_0^2 q(\bar{u}^{h,j}_{\mathrm{Re}}\lambda^{h,j}_{\mathrm{Re}} + \bar{u}^{h,j}_{\mathrm{Im}}\lambda^{h,j}_{\mathrm{Im}})\right) d\hat{\Omega}_n.$$

to order $\mathcal{O}(h^2)$, which is consistent with the discretization error of the PDEs.

3.2 Reduced-Space Method for Continuous Design The derivation in the preceding section shows that we can write the finite-dimensional approximation of (2.4) as

$$\underset{v\in[0,1]^N}{\text{minimize}} \quad \hat{J}^h(v) = \frac{1}{2|\Theta(s)|}\sum_{j=0}^{s}\|S^h_{\theta_j}(v) + \bar{u}^{(j)}_h\|^2_{2,D_0}, \tag{3.5}$$

where $S^h_{\theta_j}(v)$ is the solution operator for the FEM mesh of size h given by the system (3.3) with angle θ_j. The derivation of the reduced gradient, $\nabla_v J^h(v)$, is given in (3.1), and we apply a reduced-space optimization approach using a quasi-Newton approximation of the Hessian.

We note that the structure of the discretized state and adjoint equations (3.3) and (3.4), respectively, implies that this optimization problem is nonconvex, because the state equations are bilinear in v and u. We investigate the effect of this nonconvexity in Section 5.

4 Solving the Mixed-Integer Design Problem The finite-dimensional approximation of the nominal and uncertain MIPDECO (2.4) and (2.5), respectively, become finite-dimensional pure integer nonlinear optimization problems:

$$\underset{v\in\{0,1\}^N}{\text{minimize}} \quad \hat{J}^h(v) = \frac{1}{2}\|S^h_\theta(v) + \bar{u}_h\|^2_{2,D_0} \tag{4.1}$$

and

$$\underset{v\in\{0,1\}^N}{\text{minimize}} \quad \hat{J}^h(v) = \frac{1}{2|\Theta(s)|}\sum_{j=0}^{s} \|S^h_{\theta_j}(v) + \bar{u}^{(j)}_h\|^2_{2,D_0}, \tag{4.2}$$

respectively, where $S^h_\theta(v)$ is the solution operator defined in (3.3).

The structure of (4.1) and (4.2) involving the solution operators $S^h_\theta(v)$ makes it difficult to apply the standard MINLP solvers (e.g., [1, 4, 13]) that require analytic expressions for all the functions. One approach might be to include the discretized PDEs (3.3) and (3.4) directly as constraints. However, we found on other MIPDECOs that such an approach does not result in an MINLP that can be solved by modern MINLP solvers. Hence we consider a heuristic approach as described next.

Our approach for solving the MIPDECOs, (4.1) and (4.2), is a two-phase method. We first solve a relaxation, (2.19) and round its solution. We then apply a discrete steepest-descent trust-region approach to improve this rounded solution. Our approach builds on the method in [10] and can be interpreted as a rounding heuristic followed by repeated application of local branching [9, 14]. Unlike local branching, however, we use only first-order information to solve a sequence of approximations enforcing descent from one iteration to the next. As a result, each trust-region subproblem requires the solution of the discretized forward and adjoint PDEs, (3.3) and (3.4), respectively, making it computationally efficient for MIPDECOs. Moreover, the trust-region problem itself can be solved efficiently as a knapsack problem.

4.1 Rounding Heuristic After solving the relaxation, we use a rounding heuristic with rounding threshold τ,

$$R_\tau(v_n) = \begin{cases} 1 & \text{if } v_n \geqslant \tau \\ 0 & \text{otherwise.} \end{cases} \tag{4.3}$$

A popular rounding heuristic is $\tau = 0.5$. However, we chose $\tau = 0.8$. We have observed in our numerical computation that using this value of τ yields an objective value that is at least 10 percent lower than using $\tau = 0.5$.

4.2 Steepest-Descent Trust-Region for MIPDECO Here we describe our steepest-descent trust-region approach to improve the rounded solution. The trust-region algorithm can use any feasible $v \in \{0,1\}^N$ as a starting guess. However, we use the rounded solution of the continuous relaxation (2.19). On the kth iteration, the algorithm tries to produce a better design by changing at most Δ_k elements of $v^{(k)}$ to improve the cloaking capability of our design. The algorithm terminates once $\Delta_k < 1$, which means that no local improvement could be found and reducing Δ_k further would not yield a better point. The algorithm is shown in Algorithm 4.1.

We interpret Algorithm 4.1 as a trust-region method for solving MIPDECOs. We choose the l_1-norm trust region because it is equivalent to the hamming distance between v and $v^{(k)}$, and hence floor (Δ_k) corresponds to the maximum number of components of v that can change from their current value $v^{(k)}$. One can see easily that the trust-region constraint $\|v - v^{(k)}\|_1 \leqslant \Delta_k$ is equivalent to the following affine constraint,

$$\sum_{\substack{i=0 \\ v_i^{(k)}=0}}^{N} v_i + \sum_{\substack{i=1 \\ v_i^{(k)}=1}}^{N} (1 - v_i) \leqslant \Delta_k, \tag{4.4}$$

Algorithm 4.1 Steepest-Descent Trust-Region Algorithm.

Given initial trust-region radius $\Delta_0 = \bar{\Delta} \geqslant 1$ and initial guess $v^{(0)} \in \{0,1\}^N$
Select an acceptance step parameter $\bar{\rho}$, and set $k \leftarrow 0$
Evaluate the objective function $\hat{J}_h^{(k)} = \hat{J}^h(v^{(k)})$ and the gradient $g_h^{(k)} = \nabla_v \hat{J}^h(v^{(k)})$
while $\Delta_k \geqslant 1$ **do**
  Solve the trust-region (knapsack) subproblem for $\widehat{v}$:

$$\begin{aligned} \widehat{v} = \underset{v}{\text{argmin}} \quad & g_h^{(k)^T}\left(v - v^{(k)}\right) + \hat{J}_h^{(k)} \\ \text{subject to} \quad & \|v - v^{(k)}\|_1 \leqslant \Delta_k \\ & v \in \{0,1\}^N \end{aligned}$$

  Evaluate the objective $\hat{J}_h(\widehat{v}, u(\widehat{v}))$ by solving state equations with $\widehat{v}$
  Compute the ratio of actual over predicted reduction: $\rho_k = \frac{\hat{J}^{(k)} - \hat{J}(\widehat{v}, u(\widehat{v}))}{-\left(g^{(k)}\right)^T\left(\widehat{v} - v^k\right)}$
  if $\rho_k > \bar{\rho}$ **then**
    Accept the step: $v^{(k+1)} = \widehat{v}$, and evaluate the gradient $g^{(k+1)} = \hat{J}'(v^{(k+1)})$
    if $\|v^{(k+1)} - v^{(k)}\|_1 = \Delta_k$, **then** increase the trust-region radius $\Delta_{k+1} = 2\Delta_k$;
  else if $\rho_k > 0$ **then**
    Accept the step $v^{(k+1)} = \widehat{v}$, and evaluate the gradient $g^{(k+1)} = \hat{J}'(v^{(k+1)})$
    Keep trust-region radius unchanged $\Delta_{k+1} = \Delta_k$
  else
    Reject the step, set $v^{(k+1)} = v^{(k)}$, and copy the gradient $g^{(k+1)} = g^{(k)}$
    Reduce the trust-region radius $\Delta_{k+1} = \text{floor}\left(\frac{\Delta_k}{2}\right)$
  Set $k \leftarrow k + 1$

resulting in a knapsack constraint. We note that the binary knapsack problem can be solved in polynomial time. The step acceptance and step rejection criteria are taken directly from the nonlinear trust-region method; see, for example, [15].

5 Numerical Experiments In this section we describe our experience in solving the nominal cloak design (4.1) and the cloak design under uncertainty (4.2). We start by stating the common features of both experiments. We examine the convexity properties of our design problem and then present the results for the nominal and uncertain design in turn.

5.1 Experimental Setup We consider the cloaking of three different domains D_0^1, D_0^2, and D_0^3 given by

$$\begin{aligned} D_0^1 &= \{x, y \mid -0.6 \leqslant x \leqslant 0.6\ 0.7 \leqslant y \leqslant 1\} && \text{(Rectangle)} \\ D_0^2 &= \{x, y \mid 0.7 \leqslant x \leqslant 1\ 0.7 \leqslant y \leqslant 1\} && \text{(Square)} \\ D_0^3 &= \{x, y \mid (x - .85)^2 + (y - .85)^2 \leqslant (.1)^2\} && \text{(Circle)}, \end{aligned} \tag{5.1}$$

which are illustrated in Figure 2. We run all our tests using a MacOS desktop with a 4-core Intel processor working at 3.3 GHz. We use the FEniCS package in Python [2] version 2017.2.0 to solve the state and adjoint PDEs using piecewise linear basis functions, which uses PETSc [3] for the linear algebra. In addition we use the FEniCS default two-point Gauss quadrature method to build the components of the gradient. To solve the relaxation, we use the Toolkit for Advanced Optimization

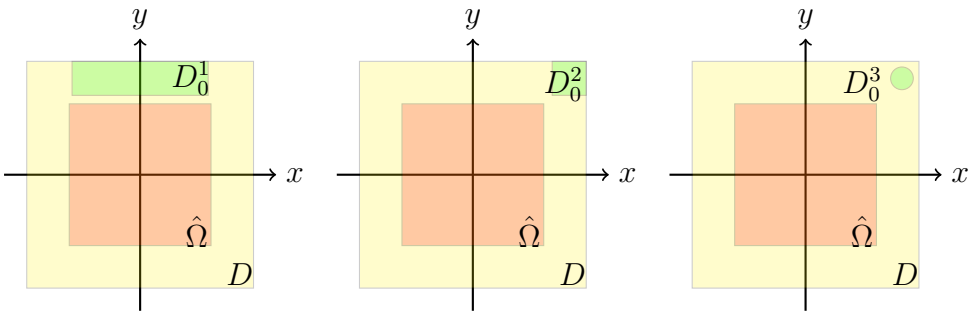

Fig. 2: Illustration of the three domains to be cloaked. The computational domain, D, is given in yellow. The domain $\widehat{\Omega}$ where the cloak is constructed is given in red. The domain that we aim to cloak is given in green for the instances D_0^1, D_0^2, and D_0^3.

(TAO) [8] with the "blmvm" solver, which is a limited-memory backtracking quasi-Newton method for solving bound-constrained problems. We use CPLEX 12.8.0.0 to solve our trust-region knapsack problem. In our trust-region method, we use $\bar{\rho} = .75$, as recommended by [15], and an initial trust-region radius of $\Delta_0 = 256$. All numerical experiments use the following set of common parameters: wave number $k_0 = 6\pi$, material constant $q = 0.75$, and cloak location $\widehat{D} \subset D$, where

$$D = \big[-1, 1\big] \times \big[-1, 1\big] \quad \text{and} \quad \widehat{D} = \left[-\frac{5}{8}, \frac{5}{8}\right] \times \left[-\frac{5}{8}, \frac{5}{8}\right]. \tag{5.2}$$

Preliminary numerical simulations indicate that a 128×128 mesh of finite elements is the best balance between an efficient solution of the state and adjoint equations and a reliable gradient evaluation. We create six test problems each for the nominal and uncertain design by taking the three cloaking regions from (5.1) and two incidence angles for each region, namely, $\theta = \frac{\pi}{4}$ and $\theta = \frac{\pi}{2}$ in the nominal design. In the case of the design under uncertainty, we consider the same two nominal angles with an uncertainty set of $\pm\frac{\pi}{4}$, giving $\theta \in \big[0, \frac{\pi}{2}\big]$ and $\theta \in \big[\frac{\pi}{4}, \frac{3\pi}{4}\big]$, respectively.

5.2 Effect of the Nonconvexity We investigate the nonconvexity of our optimal design problem by defining a parametric function $w : [0, 1] \to L^2(\hat{\Omega})$,

$$w(t)(x, y) = tw_1 + (1 - t)w_2, \quad \text{where} \quad w_k = \sum_{n=1}^{N} v_n^k \mathbb{1}_{\Omega_n \setminus \partial\Omega_n}, \text{ for } k = 1, 2, \tag{5.3}$$

for the particular choice

$$v_n^1 = \begin{cases} 1 & n \quad \text{even} \\ 0 & n \quad \text{odd} \end{cases} \quad \text{and} \quad v_n^2 = \begin{cases} 1 & n \quad \text{odd} \\ 0 & n \quad \text{even.} \end{cases} \tag{5.4}$$

It follows that $0 \leqslant w(t) \leqslant 1$, $\forall t \in [0, 1]$, and thus $w(t)$ is a feasible point for the relaxation. We then discretize the interval $[0, 1]$ into 100 discrete points, $t_1, ..., t_{100}$, calculate $w(t_i)$ for $i = 1, .., 100$, and numerically solve the PDE constraint in (2.4) using $w := w(t_i)$. Next, we evaluate the objective $J^h(w(t))$ on a 128×128 mesh and plot $J^h(w(t))$ versus t for the circle, square and rectangle geometries for $\theta = \frac{\pi}{4}, \frac{\pi}{2}$, for

a 20×20 cloak to demonstrate that the objective function is nonconvex; see Figure 3.

In all cases we see that the objective function is a nonconvex function of t. Because of this nonconvexity, the quasi-Newton method yields only a local minimum. Consequently, we cannot guarantee that the objective associated with the solution of the relaxation found is a valid lower bound on the integer solution. In fact, we observe that even the rounding step can improve/reduce the objective value.

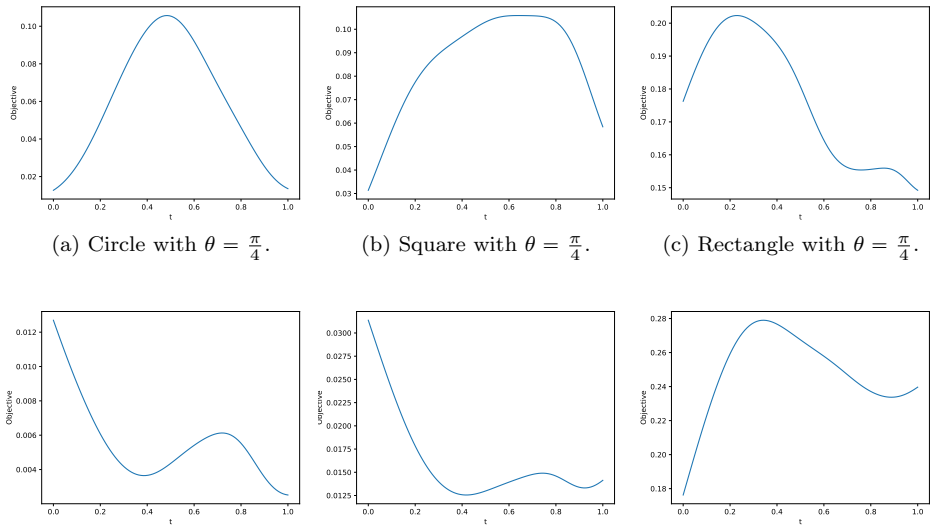

(a) Circle with $\theta = \frac{\pi}{4}$. (b) Square with $\theta = \frac{\pi}{4}$. (c) Rectangle with $\theta = \frac{\pi}{4}$.

(d) Circle with $\theta = \frac{\pi}{2}$. (e) Square with $\theta = \frac{\pi}{2}$. (f) Rectangle with $\theta = \frac{\pi}{2}$.

Fig. 3: Nonconvexity of the objective function for a single angle of attack.

5.3 Results for the Nominal Problem Next, we evaluate how well the trust-region method performs from random starting points for all cloaking domains on a 20×20 mesh and a 40×40 control mesh. For each instance, we create 25 random samples of $v \in \{0, 1\}^N$, solve for the state, and plot the corresponding objective value. We then use each of these samples v as a starting guess for our trust-region method, with $\theta = \frac{\pi}{4}$, and plot the objective at the end. The results are shown in Figure 4.

We observe that not only has the trust-region method reduced the objective function value in all cases but also that the variance of the final objective value, is significantly lower.

Next, we investigate solving the relaxation of (4.1), with TAO for the rectangular domain with $\theta = \frac{\pi}{2}$ for the 20×20 and the 40×40 control mesh (Figures 5a and 5d respectively). We note that both the objective function value (Figures 5b and 5e) and the norm of the projected gradient (Figures 5c and 5f) are reduced; in both cases, TAO reduces the projected gradient below 10^{-3}. We also note that the optimal solution for both mesh sizes is similar.

Next, we apply our rounding strategy (4.3) to obtain a rounded solution to use as a feasible starting point for our trust-region method. We have observed numerically that starting the trust-region method with an initial starting point of the rounded relaxation yields a lower objective value when compared to starting the trust-region

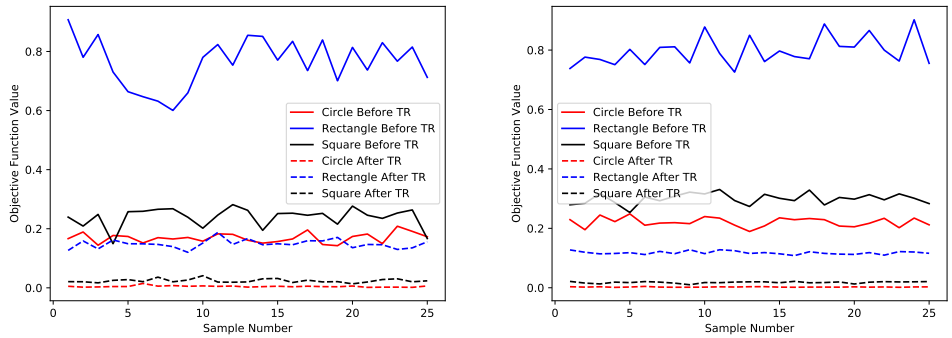

(a) 20×20 nominal. (b) 40×40 nominal.

Fig. 4: Trust-region method applied to 25 randomly generated samples for $\theta = \frac{\pi}{4}$ and three cloaking domains. The solid lines show the objective function value at initial guess and the dashed lines of the corresponding color show the objective value after the trust-region method terminated.

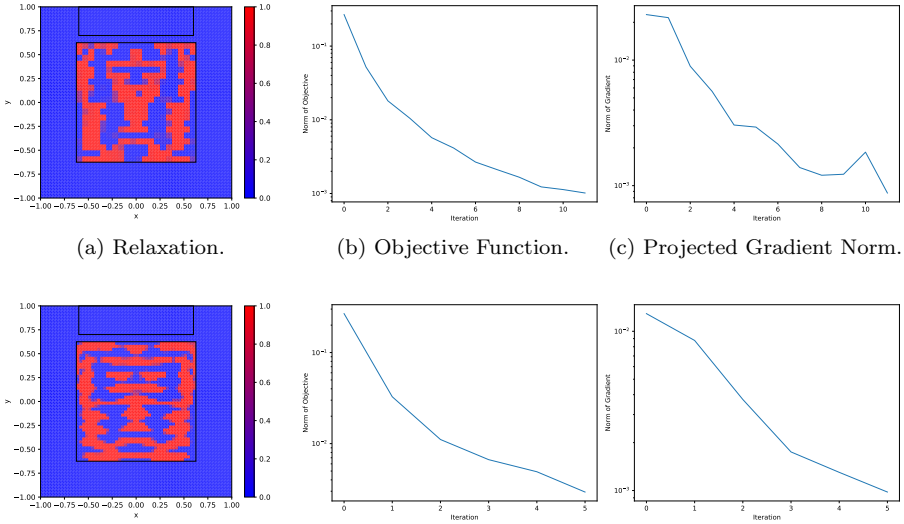

(a) Relaxation. (b) Objective Function. (c) Projected Gradient Norm.

(d) Relaxation. (e) Objective Function. (f) Projected GradientNorm.

Fig. 5: TAO relaxation results on the rectangular region with $\theta = \frac{\pi}{2}$

for 20×20 control mesh (top row) and 40×40 control mesh (bottom row).

method from a randomly generated design.

In Figures 6c and 6f we show a $\log_{10}$ plot of the scattering field, $\log_{10}(|u + \bar{u}_\theta|)$, and show that we reduce the integrand of the objective value in the region of interest to a small value. In addition, the gradient over the cloaking region, as shown in Figures 6b and 6e is small, indicating that we have likely found a local optimum to (4.1). We also observe that the final integer cloak is similar to the relaxation, which

indicates that relaxation is a good initial guess. When we compare the final discrete design in Figure 6 with the solution of the continuous relaxation in Figure 5, we note that the two designs are similar.

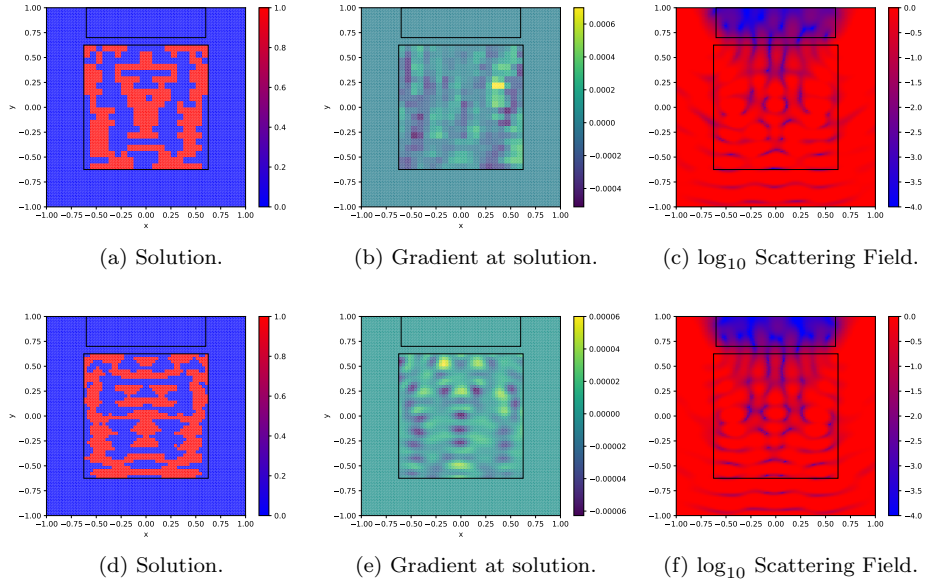

(a) Solution. (b) Gradient at solution. (c) $\log_{10}$ Scattering Field.

(d) Solution. (e) Gradient at solution. (f) $\log_{10}$ Scattering Field.

Fig. 6: Results of the trust-region method applied to the rounded relaxation for $\theta = \frac{\pi}{2}$ for cloaking domain D_0^1. The top row shows the 20×20 results, and the bottom row shows the 40×40 results.

In Figure 7 we show the progress of our trust-region method in terms of objective function values and trust-region radii as a function of iteration for the 20×20 and 40×40 control meshes. We observe that our trust-region method is successful at reducing the incumbent objective function for the small trust-region radii regime, making steady improvement.

The complete set of results for the three cloaking domains is shown in the electronic supplement SM1. In Tables 1 and 2 the first column shows the domain and the second column shows the size of the control mesh. We report the CPU time in seconds for our trust-region method in Tables 1 and 2 for the nominal angle $\theta = \frac{\pi}{4}$ and $\theta = \frac{\pi}{2}$, respectively. The tables summarize the computational effort required to solve the MIPDECO. The first three measures show the CPU time of the relaxation solve, the CPU time of the forward (state), adjoint and gradient computation, and the CPU time of the knapsack solve. The CPU time for PDEs/gradient includes computational effort required to build $w(v)$. We include this to highlight the additional computational time required going from 20×20 to 40×40 cloak elements, because of the size of each of the respective gradients.

We observe from Tables 1 and 2 that the computation time for solving the knapsack problems, denoted as MIPs, is negligible. We also observe that the number of trust-region iterations required to meet our termination condition is modest. The trust-region methods time is divided into the amount of time it takes to solve the PDEs, build the gradient, and then solve the knapsack problem. We note that the

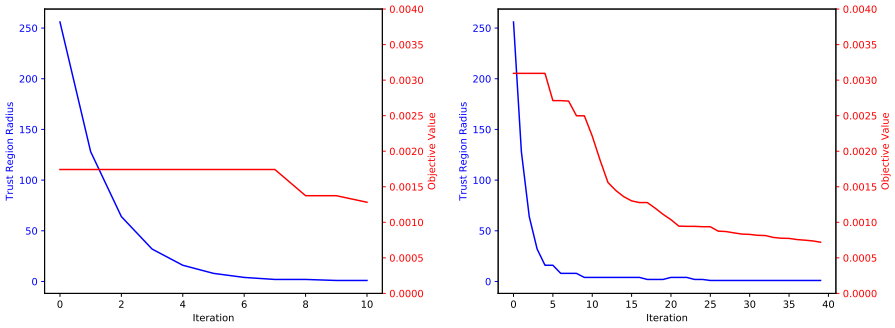

(a) 20×20. (b) 40×40.

Fig. 7: Trust-region progress for 20×20 and 40×40 control mesh.

Table 1: CPU times(s) for nominal relaxation and PDE solves, as well as trust-region computation on the 128 × 128 mesh with $\theta = \frac{\pi}{4}$.

Problem Instance		Solution CPU Time(s)			Trust-Region	Solution
Domain	Control	Relaxation	PDEs/Gradient	MIPs	Iterations	Figure
D_0^1	20 × 20	302.48	98.23	0.26	15	SM2
D_0^2	20 × 20	125.93	122.85	0.59	20	SM10
D_0^3	20 × 20	35.27	121.39	0.42	20	SM18
D_0^1	40 × 40	1497.04	420.39	0.51	20	SM6
D_0^2	40 × 40	141.06	1789.25	1.48	79	SM14
D_0^3	40 × 40	196.24	1405.30	1.42	68	SM22

number of iterations required to solve (4.1) grows only moderately as we increase the control mesh from 20×20 to 40×40, even though the design space grows exponentially.

In Table 3 we report numerical values of the objective associated with the nominal angles $\theta = \frac{\pi}{4}$ and $\theta = \frac{\pi}{2}$. The table contains three values: the relaxed objective, $\hat{J}(u^{\text{relax}})$, the rounded relaxation objective function value, $\hat{J}(u^{\text{round}})$, and the trust-region objective function value $\hat{J}(u^{\text{trust}})$. In all simulations we are able to reduce the objective for the circle and square cases to a reasonably small value. The objective associated with the rectangle is much larger by comparison, which is due to its having a larger area. We see in several cases that our trust-region method is able to reduce the objective value. We observe that the relaxed objective function value does not always give a lower bound on the solution. In fact, in some cases, simply rounding already reduces the objective function value. We believe that this behavior is a result of the nonconvexity of our problem.

5.4 Results for the Uncertainty Problem We now present our results for the design under uncertainty, (4.2). In Figure 8 we compare the design found for the 40×40 instance for a nominal angle of $\theta = \frac{\pi}{4}$ and the design found from solving the uncertainty problem for 15 angles on $\left[0, \frac{\pi}{2}\right]$ for D_0^1, D_0^2, and D_0^3. Similar results for the nominal angle of $\theta = \frac{\pi}{2}$ can be found in the electronic supplement SM1.We see a clear difference in design for the rectangle geometry.

Table 2: CPU times(s) for nominal relaxation and PDE solves, as well as trust-region computation on 128×128 mesh with $\theta = \frac{\pi}{2}$.

Problem Instance		Solution CPU Time(s)			Trust-Region	Solution
Domain	Control	Relaxation	PDEs/Gradient	MIPs	Iterations	Figure
D_0^1	20×20	76.53	60.31	0.16	11	SM26
D_0^2	20×20	41.77	84.77	0.22	17	SM34
D_0^3	20×20	31.43	89.12	0.17	18	SM42
D_0^1	40×40	202.40	917.72	1.06	40	SM30
D_0^2	40×40	86.24	671.36	0.72	41	SM38
D_0^3	40×40	56.55	872.90	0.98	50	SM46

Table 3: Objective function values for nominal problem.

Problem Instance		$\theta = \frac{\pi}{4}$			$\theta = \frac{\pi}{2}$		
Domain	Control	Relaxed Objective	Relaxed Rounded Objective	Trust Region Objective	Relaxed Objective	Relaxed Rounded Objective	Trust Region Objective
D_0^1	20×20	0.0142	0.0321	0.0168	0.0010	0.0017	0.0012
D_0^2	20×20	0.0054	0.0077	0.0052	0.0032	0.0097	0.0036
D_0^3	20×20	0.0015	0.0014	0.0011	0.0002	0.0126	0.0017
D_0^1	40×40	0.0168	0.0219	0.0163	0.0029	0.0030	0.0007
D_0^2	40×40	0.0068	0.0077	0.0032	0.0039	0.0187	0.0031
D_0^3	40×40	0.0019	0.0016	0.0010	0.0010	0.0126	0.0008

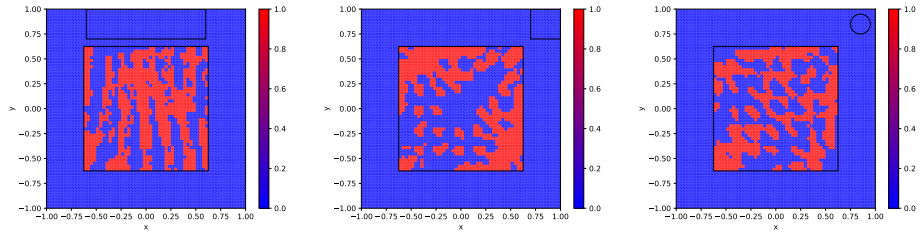

(a) Rectangle nominal. (b) Square nominal. (c) Circle nominal.

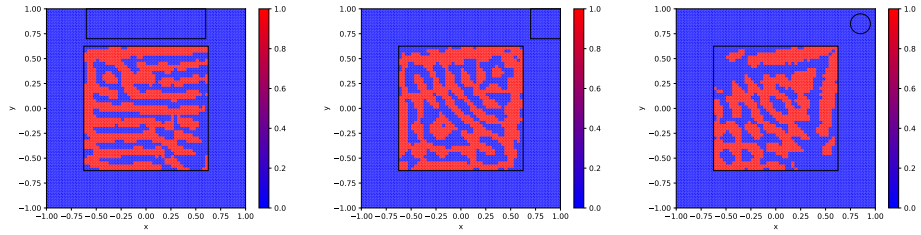

(d) Rectangle uncertain. (e) Square uncertain. (f) Circle uncertain.

Fig. 8: Cloak designs for design under uncertainty using 15 uniformly distributed $\theta \in \left[0, \frac{\pi}{2}\right]$ and for nominal angle $\frac{\pi}{4}$.

In Tables 4 and 5 we repeat the computational effort required to solved the uncertainty simulation for 15 angles. We again take $v^{(0)} = 0.5$ as a starting guess in TAO. As in the nominal case, solving the relaxation takes the most computational effort compared with the trust-region method. Even though more angles are present in the uncertainty problem, the number of trust-region iterations does not increase drastically. As in the nominal case, the computational time in the trust-region method is dominated by solving the PDEs and constructing the gradient, not by solving the knapsack problems. Another similarity is the number of iterations required by our trust-region method, which increases modestly as we go from optimizing over 20×20 integer variables to 40×40. The number of trust-region iterations is not dependent on the number of angles since we see similar iteration counts between a single angle and 15 angles. In the electronic supplement SM1 we include plots for all numerical simulations.

Table 4: CPU times(s) for uncertainty relaxation, PDE/gradient calculation and knapsack problem on 128×128 mesh for 15 angles where $\theta \in \left[0, \frac{\pi}{2}\right]$.

Problem Instance		Solution CPU Time(s)			Trust-Region	Solution
Domain	Control	Relaxation	PDEs/Gradient	MIPs	Iterations	Figure
D_0^1	20×20	1094.43	690.49	0.31	19	SM5
D_0^2	20×20	158.04	762.72	0.34	23	SM13
D_0^3	20×20	121.82	418.73	0.11	13	SM21
D_0^1	40×40	1996.71	1005.43	0.23	18	SM9
D_0^2	40×40	355.67	2444.14	0.77	44	SM17
D_0^3	40×40	306.21	2664.15	0.79	48	SM25

Table 5: CPU times(s) for uncertainty relaxation, PDE/gradient calculation and knapsack problem on 128×128 mesh for 10 angles where $\theta \in \left[\frac{\pi}{4}, \frac{3\pi}{4}\right]$.

Problem Instance		Solution CPU Time(s)			Trust-Region	Solution
Domain	Control	Relaxation	PDEs/Gradient	MIPs	Iterations	Figure
D_0^1	20×20	2093.23	430.97	0.18	17	SM29
D_0^2	20×20	137.17	430.98	0.16	17	SM37
D_0^3	20×20	135.26	361.15	0.13	14	SM45
D_0^1	40×40	2495.73	3900.51	0.91	61	SM33
D_0^2	40×40	326.36	3715.97	0.89	60	SM41
D_0^3	40×40	62.42	5986.25	1.64	105	SM49

In Table 6, we show the solution quality for the uncertainty case. We see that in many cases, similar to the single angle case, we can reduce the objective function value below the relaxed objective function value, which is due to the nonconvexity of our problem.

We also compare the nominal design to the uncertainty design over a range of angles for the circular domain. We define the function

$$f(\tilde{\theta}) = \hat{J}^h(\tilde{\theta}; v^{trust}). \tag{5.5}$$

Table 6: Objectives for uncertainty problem with 15 angles.

Problem Instance		$\theta \in \left[0, \frac{\pi}{2}\right]$			$\theta \in \left[\frac{\pi}{4}, \frac{3\pi}{4}\right]$		
Domain	Control	Relaxed Objective	Relaxed Rounded Objective	Trust Region Objective	Relaxed Objective	Relaxed Rounded Objective	Trust Region Objective
D_0^1	20×20	0.0927	0.0941	0.0902	0.0773	0.0770	0.0762
D_0^2	20×20	0.0106	0.0107	0.0083	0.0196	0.0210	0.0190
D_0^3	20×20	0.0042	0.0034	0.0028	0.0086	0.0093	0.0082
D_0^1	40×40	0.0818	0.0818	0.0077	0.0614	0.0647	0.0597
D_0^2	40×40	0.0111	0.0101	0.0071	0.0220	0.0220	0.0183
D_0^3	40×40	0.0043	0.0030	0.0017	0.0197	0.0126	0.0090

We take the solution of the trust-region method from the nominal and the uncertainty case with a given $\tilde{\theta}$, solve the state, and evaluate the objective value to obtain $f(\tilde{\theta})$. We compare the nominal design for $\theta = \frac{\pi}{4}$ with the uncertainty design found using 5, 10, and 15 angles from the interval $\left[0, \frac{\pi}{2}\right]$ on the 20×20 and 40×40 control meshes, respectively. We evaluate f on $\tilde{\theta} = \left[0, \frac{\pi}{2}\right]$ by breaking the interval into 100 sample points and then plot the resulting objective value as a function of θ, as shown in in Figure 9. We observe that the nominal design produces a lower objective value at $\frac{\pi}{4}$ when compared to the uncertain designs, which is expected. However, when we move away from the nominal angle, $\theta = \frac{\pi}{4}$, we observe that the uncertain design performs better than the nominal design. We built the nominal design to cloak for a single angle, so it makes sense that it is superior to the uncertain design at $\theta = \frac{\pi}{4}$, which covers several angles. Similarly, because the uncertain design was developed for several angles, it performs better across a range of angles.

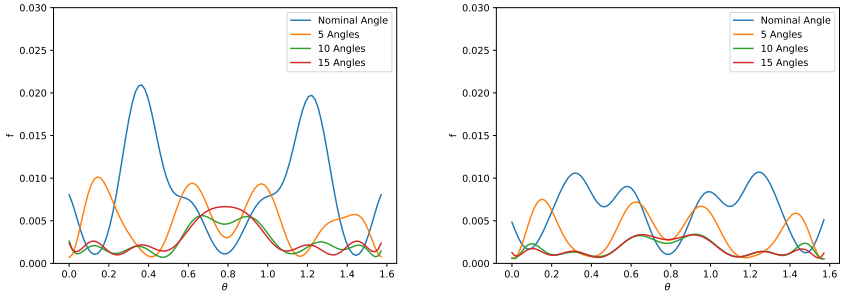

(a) Comparison 20×20. (b) Comparison 40×40.

Fig. 9: Comparison of nominal versus robust cloak design over a range of angles θ.

6 Conclusions In this paper, we introduced a trust-region method to solve MIPDECO problems. We applied our method, successfully, to construct binary electromagnetic cloaking devices that are effective at inducing electromagnetic cloaking, both for deterministic and uncertain incidence waves. The method uses tools that

are standard in the PDE optimization and mixed-integer programming communities. Our method starts by solving the relaxation, rounds that solution, and then performs a modest number of trust-region iterations. The gradient in our trust-region method is found by using techniques from PDE-constrained optimization. The integer portion of the MIPDECO problem is dealt with in the trust-region subproblem, which is a knapsack problem.

Acknowledgments We thank Alen Alexanderian, David Aspnes, Lorena Bociu, Yahya Fathi, Pierre Gremaud, and Zhilin Li from North Carolina State University and Alp Dener and Mirko Hahn from Argonne National Laboratory for helpful discussions.

REFERENCES

[1] T. Achterberg, *Scip: solving constraint integer programs*, Mathematical Programming Computation, 1 (2009), pp. 1–41.

[2] M. S. Alnæs, J. Blechta, J. Hake, A. Johansson, B. Kehlet, A. Logg, C. Richardson, J. Ring, M. E. Rognes, and G. N. Wells, *The FEniCS project version 1.5*, Archive of Numerical Software, 3 (2015), https://doi.org/10.11588/ans.2015.100.20553.

[3] S. Balay, S. Abhyankar, M. F. Adams, J. Brown, P. Brune, K. Buschelman, L. Dalcin, A. Dener, V. Eijkhout, W. D. Gropp, D. Karpeyev, D. Kaushik, M. G. Knepley, D. A. May, L. C. McInnes, R. T. Mills, T. Munson, K. Rupp, P. Sanan, B. F. Smith, S. Zampini, H. Zhang, and H. Zhang, *PETSc users manual*, Tech. Report ANL-95/11 - Revision 3.12, Argonne National Laboratory, 2019, https://www.mcs.anl.gov/petsc.

[4] P. Bonami, G. Cornuéjols, A. Lodi, and F. Margot, *A feasibility pump for mixed integer nonlinear programs*, Mathematical Programming, 119 (2009), pp. 331–352.

[5] W. Cai, U. K. Chettiar, A. V. Kildishev, and V. M. Shalaev, *Optical cloaking with metamaterials*, Nature photonics, 1 (2007), p. 224.

[6] T. J. Cui, D. R. Smith, and R. Liu, *Metamaterials*, Springer, 2010.

[7] S. A. Cummer, B.-I. Popa, D. Schurig, D. R. Smith, and J. Pendry, *Full-wave simulations of electromagnetic cloaking structures*, Physical Review E, 74 (2006), p. 036621.

[8] A. Dener, T. Munson, J. Sarich, S. Wild, S. Benson, and L. C. McInnes, *TAO 3.12 users manual*, Argonne Technical Memorandum ANL/MCS-TM-242, Mathematics and Computer Science Division, Argonne National Laboratory, revised September 2019. http://www.mcs.anl.gov/petsc.

[9] M. Fischetti and A. Lodi, *Local branching*, Mathematical Programming, 98 (2002), pp. 23–47.

[10] M. Hahn, S. Sager, and S. Leyffer, *Binary optimal control by trust-region topological steepest descent*, tech. report, Argonne National Laboratory, 2018. In preparation.

[11] J. Haslinger and R. A. Mäkinen, *On a topology optimization problem governed by two-dimensional helmholtz equation*, Computational Optimization and Applications, 62 (2015), pp. 517–544.

[12] Z. Li, Z. Qiao, and T. Tang, *Numerical Solution of Differential Equations: Introduction to Finite Difference and Finite Element Methods*, Cambridge University Press, 2017.

[13] A. Mahajan, S. Leyffer, J. Linderoth, J. Luedtke, and T. Munson, *Minotaur: A mixed-integer nonlinear optimization toolkit*, Tech. Report ANL/MCS-P8010-0817, Argonne National Laboratory, Mathematics and Computer Science Division, 2017.

[14] G. Nannicini, P. Belotti, and L. Liberti, *A local branching heuristic for MINLPs*. arXiv:0812.2188v1 [math.CO], 2008. http://arxiv.org/abs/0812.2188.

[15] J. Nocedal and S. J. Wright, *Numerical Optimization*, Springer-Verlag, New York, 1999.

[16] S. Salsa, *Partial Differential Equations in Action: From Modelling to Theory*, vol. 99, Springer, 2016.

[17] D. Schurig, J. Mock, B. Justice, S. A. Cummer, J. B. Pendry, A. Starr, and D. Smith, *Metamaterial electromagnetic cloak at microwave frequencies*, Science, 314 (2006), pp. 977–980.

[18] M. Selvanayagam and G. V. Eleftheriades, *Experimental demonstration of active electromagnetic cloaking*, Physical Review X, 3 (2013), p. 041011.

[19] F. Tröltzsch, *Optimal Control of Partial Differential Equations: Theory, Methods, and Applications*, vol. 112, American Mathematical Soc., 2010.